Available online at www.sciencedirect.com
ScienceDirect
Trans. Nonferrous Met. Soc. China 32(2022) 2648−2664

Transactions of Nonferrous Metals Society of China
www.tnmsc.cn

Effect of Si/Ti additions on physico-mechanical and chemical properties of FeNiCrCo high entropy alloys manufactured by powder metallurgy technique

Sarah HEDYA[1], Lamiaa MOHAMED[2], Ghalia GABER[3],
Omayma ELKADY[4], Hassan MEGAHED[1], Shimaa ABOLKASSEM[4]

1. Mechanical Design and Production Engineering Department,
Faculty of Engineering, Cairo University, Giza 12613, Egypt;
2. Mining, Petroleum and Metallurgical Engineering Department,
Faculty of Engineering, Cairo University, Giza 12613, Egypt;
3. Department of Chemistry, Faculty of Science (Girls), Al-Azhar University,
P.O. Box: 11754, Yousef Abbas Str., Nasr City, Cairo, Egypt;
4. Powder Technology Division, Manufacturing Technology Institute,
Central Metallurgical R&D Institute, P.O. Box. 87, Helwan 11421, Cairo, Egypt

Received 7 August 2021; accepted 18 February 2022

Abstract: $FeNiCrCoSi_x$ and $FeNiCrCoTi_x$ (x=0, 0.3, 0.6, and 0.9 wt.%) high entropy alloys (HEAs) were prepared via the powder metallurgy technique. A homogenous distribution of the elements in all alloys due to the formation of a solid solution phase is observed. The density and hardness of the prepared HEAs are improved by Si and Ti additions, compared to FeNiCrCo HEA. The wear rate of the prepared alloys was studied at different loads and the results indicate that the alloys that contain 0.3 wt.% Si and 0.9 wt.% Ti have the lowest wear rates. X-ray diffraction, SEM, and EDX were used to understand the phases, grain sizes, and microstructures in different investigated HEAs. The effects of Si and Ti content on the corrosion behavior and surface morphologies of sintered $FeNiCrCoSi_x$ and $FeNiCrCoTi_x$ HEAs were studied by immersion in H_2SO_4, HNO_3, and HCl solutions. Uniform corrosion and localized pitting are observed in different sizes in the corrosive media used. Because of the smaller pit size and the reduced pit density, the $FeNiCrCoSi_{0.3}$ HEA has an excellent microstructure.

Key words: $FeNiCrCoSi_x$ alloy; $FeNiCrCoTi_x$ alloy; high entropy alloys; powder metallurgy; corrosion behavior

---

1 Introduction

High entropy alloys (HEAs) are a novel class of complex materials that were discovered near the center of the diagram phase, and they showed exceptional performance compared to the classical alloys. The HEAs are a mixture of five or more elements in an almost equiatomic composition with a high entropy effect. They have a single solid solution phase with a high entropy rather than the intermetallic compounds [1]. The HEAs have many unique combinations of properties, such as good thermal stability, distinct electrical characteristics, and excellent resistance to corrosion and wear [2−8]. Taking the CoCrFeMnNi equiatomic alloy as an example, it has a crystalline structure of the FCC having an ultra-ductility, but a low strength [1,9]. It also has excellent mechanical properties and fracture toughness at cryogenic temperatures, but its

---

Corresponding author: Lamiaa MOHAMED, E-mail: lamiaa.zaky@cu.edu.eg
DOI: 10.1016/S1003-6326(22)65973-9

strength at room temperature is low [10,11]. The Si addition affects the $AlCoCuCrFeNiSi_x$ alloy structure reported by KUMAR et al [12]. To understand the alloying behavior, the phase formation of the current HEAs was evaluated by X-ray diffraction (XRD). The XRD pattern results demonstrated that the increase of Si supports the creation of a BCC structure. The increase of Si content in $Al_{0.5}CoCrCuFeNiSi_x$ (x=0, 0.4, and 0.8) encourages the formation of BCC phase compared to FCC structure [13]. As a result of high negative enthalpy of mixing Si with other elements, a significant increase in wear resistance is attributed to the effect of the increase of Si content. The experimental findings were also consistent with the theoretical structure prediction based on mixing entropy, atomic size mismatch, enthalpy mixing, concentration of valence electrons, difference in electronegativity and entropy mismatch [12]. It is evident from the diffraction pattern that the formation of the BCC structure was more preferred than that of the FCC phase, with the increase in Si content from x=0 to 0.9%. The superiority of the standardized BCC structure can also be verified by the theoretical research carried out [14]. The value of the enthalpy of mixing becomes more negative as the Si content increases. This also points to the promotion of the formation of BCC structure [15]. Decreasing the density and changing the XRD pattern by increasing milling time may be due to the crystal size refinement, high lattice strain and the solid solution formation [16].

To evaluate the impact of Si content on the microstructures, mechanical properties, and helium irradiation resistance of the NiCoCr-based alloys, a number of $NiCoCrSi_x$ (x=0, 0.1, 0.2, and 0.3) medium-entropy alloys were synthesized. The findings indicate that when the Si content is in the range of 0−6.25 at.%, the alloys exhibit a single FCC structure, while phase decomposition occurs as the Si content increases further (~9 at.%). $NiCoCrSi_{0.2}$ demonstrated an increase in strength without losing ductility compared to NiCoCr. Both yield strength and ultimate tensile strength were increased, respectively, from 438 to 599 MPa and from 921 to 1032 MPa, while ductility remained as high as ~50% [17]. Because of its high strength and positive impacts, Si is widely used in twinning-induced plasticity (TWIP) of steels [18,19].

Ni, Co, Cr, and Fe elements have very close atomic radius values and exist in $Ni_{1.5}Co_{1.5}CrFeTi_x$ HEA. However, Ti possesses a much larger atomic size with respect to the former elements. It is therefore intuitive that Ti concentration will largely dictate the extent of solid solution strength, which should be advisably kept as high as possible. Increasing the Ti content will inevitably result in the formation of thermodynamic intermetallic phases, which decreases the solid solution strengthening effect. In order to probe the effect of Ti concentration, the change that occurred in the mechanical properties as well as phase composition and Ti partitioning effects, the $Ni_{1.5}Co_{1.5}CrFeTi_x$ alloys with x=0.3, 0.5, and 0.7 were evaluated. To prevent the segregation effects that may occur during the casting of such complex systems and the forming of coarse-grained microstructures, an alternative powder metallurgical manufacturing route of mechanical alloying and spark plasma sintering was used. The latter process enables us to produce fine-grained materials and to study their properties without the need for time- and energy-consuming additional hot and cold-working processes, which are sometimes required for cast materials [20].

This work aims to study the effects of Si/Ti additions on the properties of the sintered $FeNiCrCoM_x$ HEAs to be suitable as a catalyst, anti-radiation and functional materials. It also aims to investigate the density, microstructure, phase identification, hardness and wear of the fabricated $FeNiCrCoM_x$ HEA prepared with the powder metallurgy technique by different additions of Si and Ti, where x=0, 0.3, 0.6 and 0.9 wt.%, as well as the corrosion behavior of these HEAs in H_2SO_4, HNO_3 and HCl solutions by studying the surface morphology of the corroded HEAs with scanning electron microscopy (SEM) and energy dispersive X-ray analysis (EDX).

2 Experimental

2.1 Fabrication of sintered HEAs

Pure powders of Fe, Ni, Co, and Cr were mixed together as the FeNiCrCo HEA to contain an equiatomic composition, and then Si/Ti was added by 0.3, 0.6, and 0.9 wt.% to fabricate different HEAs with different compositions. The six kinds of powders were characterized by scanning electron microscopy (SEM) to identify their shape and particle size before mixing together. The powders were mechanically milled in a ball mill using a ball to powder ratio of 7:1 for 8 h at a speed of 350 r/min. The ball material is zirconia to reduce contamination. The mixed powders were pressed by a hydraulic press with a 520 MPa load, and then sintered in a tube furnace at a temperature of 1200 °C for 1 h in an argon atmosphere.

2.2 Characterization of sintered HEAs

The density and porosity were measured for the investigated HEAs. The Archimedes density of a sintered sample was measured using water as the floating liquid by applying Eq. (1) [21]:

$$\rho_{\mathrm{Ar}}=W_{\mathrm{a}}/(W_{\mathrm{a}}-W_{\mathrm{w}}) \tag{1}$$

where W_a and W_w are the masses of the sample in air and in water, respectively. The densification percentage (D_R) was calculated [21,22]:

$$D_{\mathrm{R}}=(\rho/\rho_{\mathrm{th}})\times 100\% \tag{2}$$

where ρ is the used density and ρ_{th} is the theoretical density.

The porosity percentage (P) was calculated from Eq. (3) [21,22]:

$$P=[(\rho_{\mathrm{th}}-\rho)/\rho_{\mathrm{th}}]\times 100\% \tag{3}$$

The phase composition and microstructure of sintered HEAs were estimated using X-ray diffraction (XRD), scanning electron microscopy (SEM), and energy dispersive X-ray analysis (EDX). For microstructure examination, samples were ground with emery paper up to 1000 grit then polished by alumina paste with 0.3 μm. Finally, the samples were etched in 10 mL HNO_3 (70% nitric acid + 30% water), 10 mL HF and 10 mL distilled water. Hardness was evaluated by using Vickers micro hardness by taking the average of 5 readings in 5 different spots at 500 g for 15 s. Also, the wear rates of the fabricated HEAs with dimensions of 8 mm × 8 mm × 12 mm were studied using pin-on-ring tribometer with SiC ring of 73 mm in diameter, by applying 5, 10, and 15 N at the velocity of 250 r/min for 15 min.

2.3 Corrosion behavior of sintered HEAs

The sintered HEAs were ground with SiC paper up to 1000 grit, then cleaned with ethanol, deionized water, and acetone, and eventually dried in air. The specimen surface was masked with tape, exposing 0.785 cm^2 area to different electrolytic solutions at room temperature. During the mass reduction estimations, $FeNiCrCoSi_x$ and $FeNiCrCoTi_x$ HEAs (x=0, 0.3, 0.6, and 0.9 wt.%) coupons are weighted (W_1) and suspended completely in three acidic media, namely 10% H_2SO_4, 10% HNO_3, and 10% HCl solutions, with a volume kept at 50 mL. The coupons were retrieved after 24, 48, 72, 96, and 120 h, washed with distilled water, dried with acetone, and reweighed (W_2). The optimum immersion time with the relatively larger mass-loss was adopted. It specified the initial total surface area of the sample (making corrections in the areas associated with the mounting holes) and the mass lost during the experiment. The average corrosion rate was obtained using Eqs. (4) and (5) as follows [23]:

$$\Delta W=W_1-W_2 \tag{4}$$

The corrosion rate (R_C) of $FeNiCrCoSi_x$ and $FeNiCrCoTi_x$ (x=0, 0.3, 0.6, and 0.9 wt.%) in different acidic solutions for 120 h tested at room temperature (~20 °C) can be calculated [24,25]:

$$R_{\mathrm{C}}=\frac{\Delta W\cdot K}{A\cdot t\cdot D} \tag{5}$$

where K is a constant (8.76×10^4), t is the time of exposure in h, A is the area in cm^2, ΔW is the mass loss in g, and D is the density in g/cm^3 (for FeNiCrCo, $FeNiCrCoSi_x$ and $FeNiCrCoTi_x$ with x= 0.3, 0.6 and 0.9 wt.%). The density of HEAs was calculated based on the elemental density. The corroded HEAs with different compositions were characterized by SEM morphologies and EDX analysis.

3 Results and discussion

3.1 Powders characterization

The Fe, Ni, Cr, Co, Si, and Ti powders used in the fabrication of HEAs with purities of 99.5%, 99.2%, 99.8%, 99.7%, and 99.5%, respectively, are characterized by SEM images to estimate the purity, particle size, and shape, as shown in Fig. 1, which indicates that Co has a particle size of 2−5 μm, Ni has a particle size of 0.5−1.11 μm, Fe has an irregular shape of 20 μm, while Cr has a particle size of 2−20 μm, Si has a particle size of 2−30 μm and Ti has a particle size of 1−25 μm. The Co, Ni, and Cr particles show a sponge-like shape.

The powders of the different HEAs were mechanically mixed together in a ball mill. The chemical composition of different HEAs prepared is tabulated in Table 1.

3.2 Characterization of sintered FeNiCrCoM$_x$ HEAs

3.2.1 Density

The relative densities of the sintered HEAs are provided in Table 2, where the maximum densification is recorded at 0.3 wt.% Si addition. The density increases by Si addition of 0.3 wt.%, but with increasing the Si content more than 0.3 wt.%, a slight decrease in the density of the prepared alloys is observed. Although the relative density of 0.3 wt.% Si sample is higher than that of 0.6 wt.% and 0.9 wt.% Si samples, which are 96.8%, 94.7%, and 93.1%, respectively, all of the three alloys have higher densification than FeNiCrCo HEA, which has a relative density of 90.5%. Because the Si element has a strong interaction with other elements, the strength increases along with maintaining a good plasticity [26]. The addition of 0.3 wt.% Si, with its smaller atomic radius than the other elemental components, enhances the filling of internal voids with Si, so the density increases.

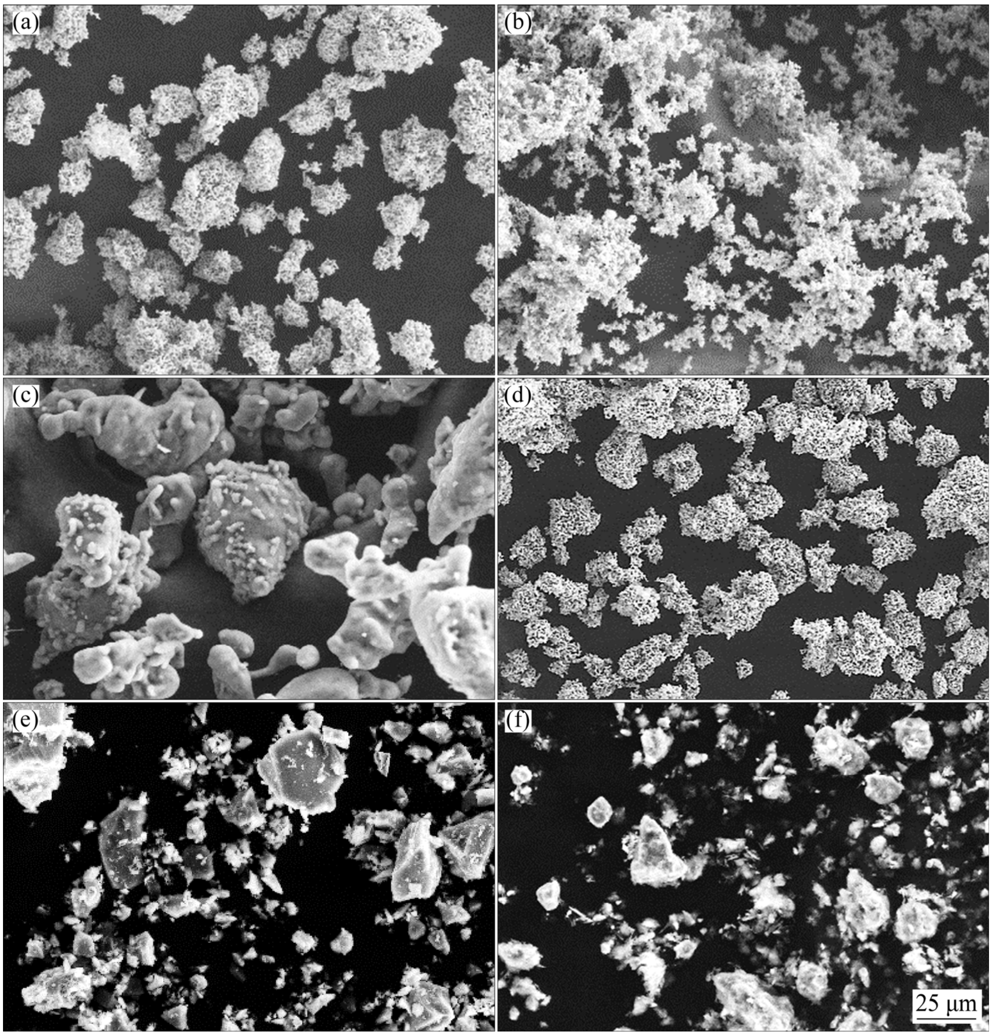

Fig. 1 SEM micrographs of Co (a), Ni (b), Fe (c), Cr (d), Si (e) and Ti (f)

Table 1 Chemical compositions of FeNiCrCoM$_x$ HEAs with different ratios of M (Ti or Si) (wt.%)

HEA	Fe	Ni	Cr	Co	M (Ti or Si)
FeNiCrCo	23.99	27.2	21.6	27.2	0
FeNiCrCoM$_{0.3}$	24	27.05	21.6	27.05	0.3
FeNiCrCoM$_{0.6}$	23.84	26.96	21.63	26.96	0.6
FeNiCrCoM$_{0.9}$	23.8	26.9	21.4	26.9	0.9

Table 2 Relative density of FeNiCrMoM$_x$ HEAs with different additions of M (Ti or Si)

x/wt.%	Relative density/%	
	FeNiCrMoTi$_x$	FeNiCrMoSi$_x$
0	90.5	90.5
0.3	90.9	96.8
0.6	91.1	94.7
0.9	92.3	93.1

However, with more Si additions, excess Si atoms are aggregated at the grain boundaries, which decreases the density. Also, with increasing the addition of Si, the density decreases due to the lower density of Si (2.3 g/cm^3) compared to the density of the other elements. On the other hand, the slight decrease in density with increasing Si amount may be due to the presence of some cracks and agglomerations, which is clearly shown in the SEM image. Also, during the sintering process, some Si atoms gather with each other, leading to grains growing and contact with each other and, hence, reducing the relative density [27].

The effect of Ti additions is that Ti is a ductile phase with a high rate of plasticization. Therefore, the Ti will not act as a milling medium. Density is increased, most likely due to the reduction of porosity and the incorporation of a high-density element [28]. Also, after sintering at 1200 °C, the formation of β titanium between 1170 and 1330 °C, leads to high ductility, weldability, and corrosion resistance for Ti, which improves the density by increasing Ti additions. Because the atomic radius of Ti is so close to that of other elements in the investigated HEA, different Ti additions cause a lower density than Si additions [29].

3.2.2 Phase structure and microstructure

Figure 2 shows the phase structure of FeNiCrCo, FeNiCrCoSi$_x$ and FeNiCrCoTi$_x$ (x=0.3, 0.6, and 0.9 wt.%) HEAs. In the case of FeNiCrCo, there are sharp peaks corresponding to FCC phase that is rich with Co_3Fe_7, FeNi and $Ni_{2.9}Cr_{0.7}Fe_{0.36}$ phases as indicated by XRD analysis, which are formed during the sintering process owing to the good solubility between them. Weak peak from chromium oxide is also observed but, with a very small intensity. By increasing Si or Ti content, they contain phases which agglomerate together leading to the separation of some amounts of Cr from FCC phase and the formation of Cr_2O_3, and hence, the peaks appear clearly [8].

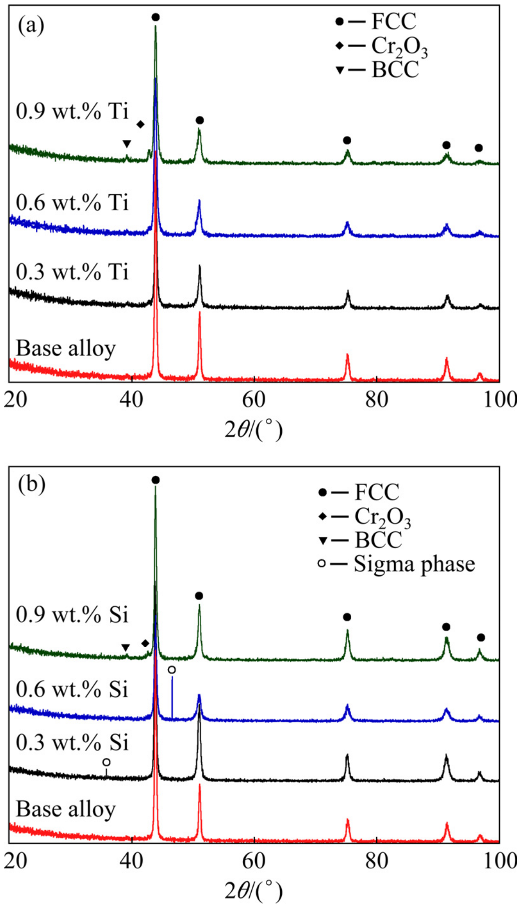

Fig. 2 XRD patterns for sintered FeNiCrCoM$_x$ alloy (x=0, 0.3, 0.6, and 0.9 wt.%): (a) M=Ti; (b) M=Si

For samples containing Si particles, there are small peaks corresponding to BCC phase, which has a strong effect on the mechanical properties of the specimens. Si atom can replace Fe, Co, Ni and Cr on the expense of the formed FCC. Consequently, the intensity of FCC phase is decreased, and peaks corresponding to BCC phase appear [27]. Also, disappearance of chromium oxide peaks can be observed due to the controlled milling process and sintering under argon atmosphere which protect the metals from any oxidation. In addition, the presence of sigma phase is detected by XRD analysis which has a great effect on the improvement of mechanical properties for 0.3 and 0.6 wt.% Si samples. Only the FCC phase and a minor peak for the BCC phase are present in FeNiCrCoTi$_x$ HEAs, which has an impact on their mechanical properties.

Microstructure investigation is vital to assessing the distribution, particle size, and shape of the constituent elements; all these parameters have a great influence on both mechanical and physical properties. Figures 3 and 4 show the SEM microstructures of the sintered FeNiCrCoTi$_x$ and FeNiCrCoSi$_x$ (x=0, 0.3, 0.6, and 0.9 wt.%) HEAs at 1200 °C for 1 h. Figure 3(a) represents the sintered FeNiCrCo HEAs without any additions of Si or Ti, where there are two phases appearing. The gray phase represents all the mixed elements, the dark gray phase represents the FCC phase formed, and the pores appear as black spots. However, the XRD appears in one phase only because the second phase has a small amount to be detected. The highest density sample with low porosity for FeNiCrCoSi$_x$ HEAs is 0.3 wt.% Si, as shown in Fig. 4(b), while the lowest pore percentage for Ti alloy samples is 0.9 wt.% Ti, as shown in Fig. 3(d).

The gray phase represents the four alloying elements Fe, Ni, Cr and Co that are mixed and mechanically alloyed. The second phase is the dark gray that belongs to the formed FCC phase while the dark black shows the pores. The EDX analysis was indicated in two spots in different areas. Spot 1 contains 31.22% Fe, 26.22% Ni, 16.98% Cr and 25.58% Co, while Spot 2 represents 23.34% Fe, 24.78% Ni, 22.95% Cr and 28.85% Co.

The grain boundary appears strongly by increasing Si content. It can be seen from the microstructure that the samples are fully densified as pores can rarely be seen. It can be observed that the structure is homogenously distributed and the phase is dispersed finely [30]. Also, an increase in the grain size by increasing Si content is obviously seen [31]. The sintered FeNiCrCoTi$_x$ HEAs have a gray phase, which represents the four constituent elements, and a small percentage of Ti elements, which represents the FCC phase. The dark gray phase contains a high concentration of Ti elements, resembling the BCC phase in the form of a lamellar shape, and finally, black spots represent pores. All phases are homogenously distributed among each other. FeNiCrCoSi$_x$ alloys contain a sigma phase in the case of 0.3 wt.% Si and 0.6 wt.% Si, as indicated by XRD analysis. This sigma phase is formed due to the mixing enthalpy of Si-HEAs, which is more negative between Fe and Cr, explaining the high mechanical and physical properties of these HEAs. However, in the case of Ti, the mixing enthalpy between Ti and Ni is highly negative, so, they tend to form intermetallics [32]. The spot EDX analysis of the sintered HEAs is represented in Tables 3 and 4.

3.2.3 Hardness

Table 5 lists the hardness values of FeNiCrCo HEA with Si/Ti additions. Three phenomena are observed. First is the increase of hardness values by

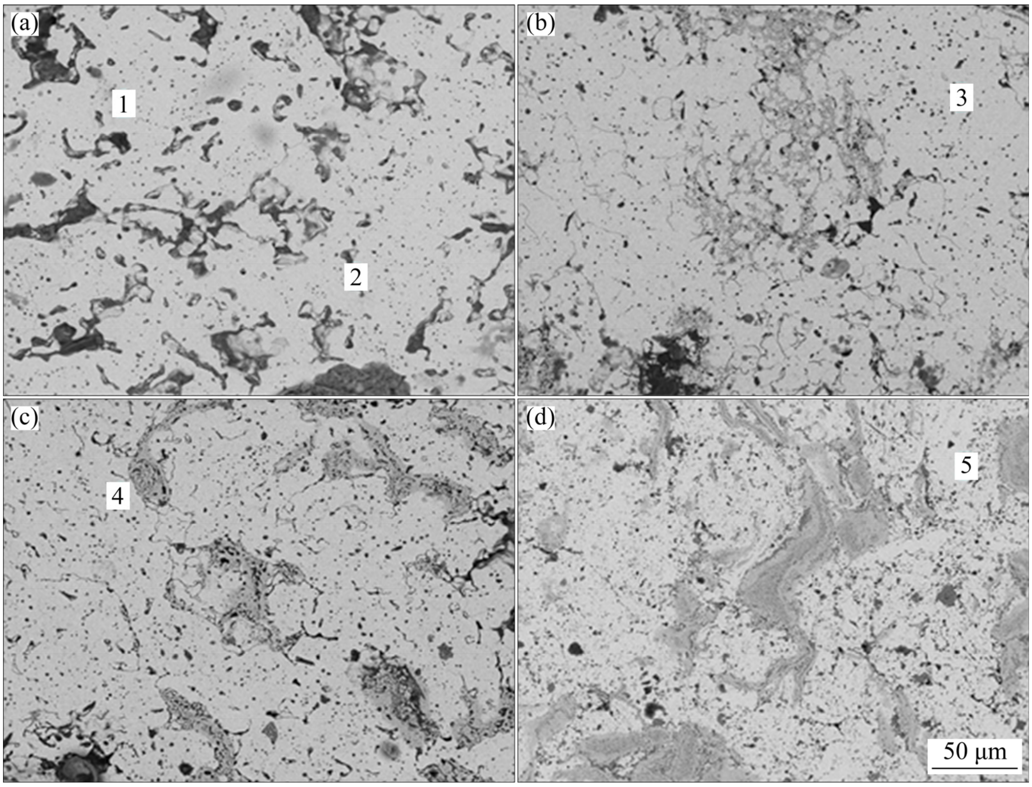

Fig. 3 SEM images of sintered FeNiCrCoTi$_x$ alloy: (a) x=0; (b) x=0.3 wt.%; (c) x=0.6 wt.%; (d) x=0.9 wt.%

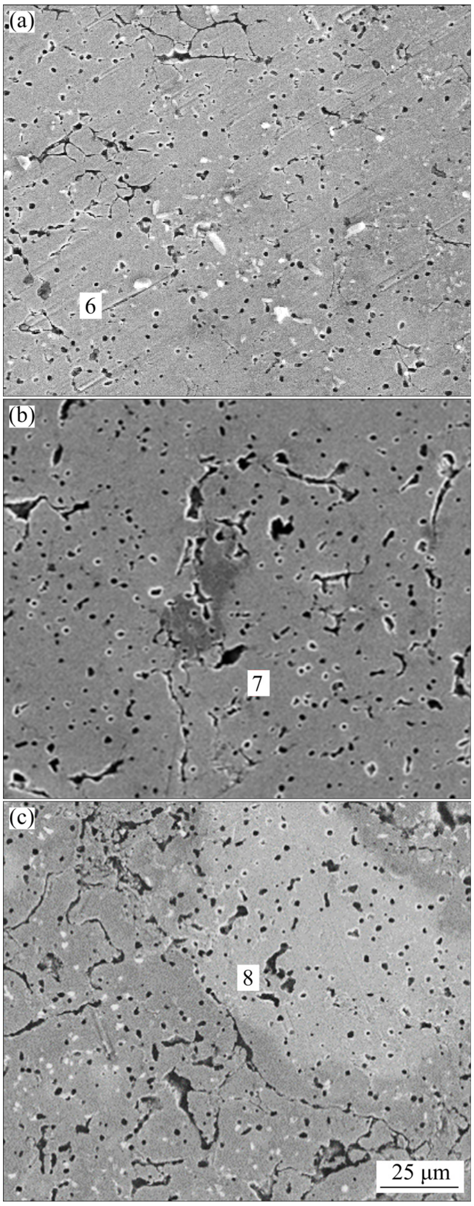

Fig. 4 SEM images of sintered FeNiCrCoSi$_x$ alloy: (a) x=0.3 wt.%; (b) x=0.6 wt.%; (c) x=0.9 wt.%

Table 3 EDX analysis results for FeNiCrCoTi$_x$ HEAs (wt.%)

Element	Spot 3	Spot 4	Spot 5
Ti	0.24	0.66	0.88
Fe	18.99	22.08	22.02
Ni	31.57	30.12	29.13
Cr	13.32	17.22	17.04
Co	35.88	29.91	30.93

Table 4 EDX analysis results for FeNiCrCoSi$_x$ HEAs (wt.%)

Element	Spot 6	Spot 7	Spot 8
Si	0.49	0.7	1.2
Fe	26.03	26.35	22.44
Ni	23.27	23.89	19.51
Cr	24.52	22.87	37.35
Co	25.69	26.19	19.5

Table 5 Hardness values of FeNiCrCoM$_x$ HEAs with different additions of M (Ti or Si)

x/wt.%	Hardness (HVN)	
	FeNiCrCoTi$_x$	FeNiCrCoSi$_x$
0	77	77
0.3	93	189
0.6	105	142
0.9	111	135

increasing Si addition up to 0.3 wt.%, and then hardness decreases by increasing Si up to 0.9 wt.%. The second phenomenon is the gradual increase of the hardness values by increasing Ti content. The third one is the higher hardness value of Si alloy samples than Ti ones. All FeNiCrCoSi$_x$ specimens have higher hardness than FeNiCrCo HEA, which is in agreement with the densification results. The improvement may be attributed to the solid solution formation that leads to a higher strength. The hardness is influenced by the distortion caused by the elements with a large atomic radius in the lattice, which contributes to the hardness. The second is the new phase produced in the microstructure, which has a major impact on the value of the hardness. Alloys with the FCC structure usually show lower hardness, whereas those with the BCC structure show higher levels of hardness. Moreover, depending on the enthalpy relationship with each other, the elements in the HEAs form hard intermetallic phases, which enhance the hardness. The low hardness of FeNiCrCo alloy can be due to its lack of hardening effects and the FCC structure. Increasing the Si addition leads to dramatic increase in hardness due to the formation of a BCC phase that has a positive effect on hardness as it is a hard phase that gives strength to the alloy. Si is an excellent BCC stabilizer [33]. Furthermore, as the Si content increases, the distribution of hardness values also increases. This may be due to the more homogeneous dispersion and finer size of the formed phases [30]. More homogeneous and similar hardness values have been determined because the phases are very thinly distributed. Generally, all the prepared alloys have higher hardness values than FeNiCrCo HEA, which might be due to the formation of the BCC phase and the absence of porosity.

On the other hand, the hardness of FeNiCrCoTi$_x$ rises gradually by increasing Ti additions. This may be due to the uniform distribution of Ti with the other elements. Another reason for the increase in hardness for FeNiCrCoTi$_x$ is that Mohs hardness of Ti about 6 is higher than the hardness of other elements, which increases the hardness of the alloy. Also, the addition of Ti by a small content leads to a clear decrease in grain size and an increase in volume fraction compared to FeNiCrCo HEA. This lends to an improvement in the mechanical properties of HEAs with only a slight addition of Ti as the hardness [34]. Moreover, the addition of Ti may also have a great effect on enhancing the solid solution strengthening effect [29]. However, the hardness of FeNiCrCoTi$_x$ is lower than that of FeNiCrCoSi$_x$, due to the lower densification of FeNiCrCoTi$_x$ than that of FeNiCrCoSi$_x$ HEAs.

The addition of Si promotes the occurrence of lower melting compositions and the filling of voids, which might have been observed in the SEM/EDX. This is due to internal oxidation and the formation of SiO$_2$, which is well known to occur in pores. The Ti addition effect might be due to β-formation in pure titanium. Also, Ti is one of the most reactive elements and will directly react to intermetallics or be oxidized.

3.2.4 Wear properties

The most important factors that affect the performance of any material are the wear resistance, sliding speed, loaded force, mass friction, and homogenization between the matrix and the reinforcement. The mass-losses of FeNiCrCoTi$_x$ and FeNiCrCoSi$_x$ HEAs are provided in Figs. 5(a, b). Dry sliding wear experiments have been conducted under three different loads. It can be seen that there is a considerable improvement in wear resistance by adding Si element compared to FeNiCrCo HEA. The FCC structure of the FeNiCrCo HEA and its low hardness reduce the wear resistance to a lower level than other samples, even though it collapses at greater loads. The higher wear resistance of other samples is related to the formed BCC phase that has great effect on hardness as well as wear resistance.

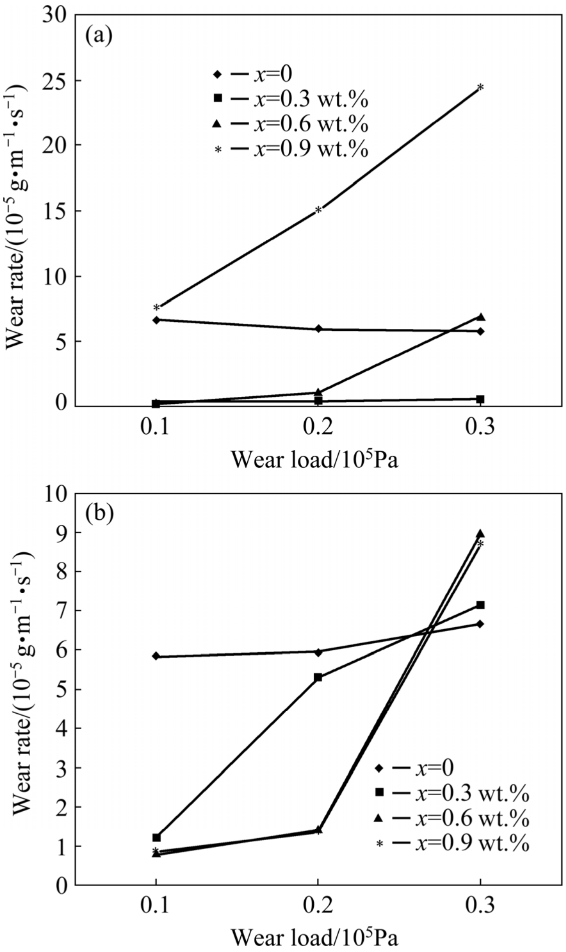

Fig. 5 Wear rates for sintered FeNiCrCoM$_x$ HEAs (x=0, 0.3, 0.6, and 0.9 wt.%) at 1200 °C: (a) M=Si; (b) M=Ti

However, mass-loss is increased by increasing the applied load to all samples and by increasing Si content. In several studies, this result has been seen and predicted. The decrease in wear rate occurs only under extreme conditions, such as the lubricating effect of the oxide film formed, which is called a tribo-layer, under high frictional heating conditions by increasing the load. Actually, the increase in the load increases the wear losses, because the abrasive ball creates a greater impact on the sample surface by increasing the applied load. The applied load contributes more to the ball's sinking on the sample surface. At the same time, the sample surface becomes more deformed and material losses increase due to the continuous sliding motion. Also, in the case of 0.3 wt.% Si HEA, the wear rate is nearly unchanged for all loads compared to the other samples. Si metal has good resistance to wear, so adding it because of its lower density than the other constituents causes it to float on the alloy surface, which enhances the wear resistance. Also, an addition of Si to FeNiCrCo HEA increases the hardness, as recorded in Fig. 5. The sample that contains 0.3 wt.% Si has the lowest wear rate due to its highest hardness. Adding an element having a high hardness and a low density, such as Si, improves its resistance to wear. In addition, the homogenous distribution of all the particles is seen from the microstructure. Moreover, as indicated by density measurement and as approved by SEM image [30], 0.3 wt.% Si HEA has the highest density, highest hardness, and lowest porosity. In the case of $FeNiCrCoTi_x$ HEAs, it can be seen that the specimens with higher hardness have higher wear resistance, and the wear rate increases with increasing load. In FeNiCrCo HEA, the wear rate is higher than in HEAs with Ti addition, but the increment rises more steeply. So, there may be another factor affecting the wear rate and the mass-loss, which is the performance of the materials during the test. The decrease in wear rate by increasing Ti additions may be due to the formation of the oxide film during the test as a result of the friction process. Ti is a very active element toward oxygen, leading to the formation of TiO_2 with higher surface stability. Hence, the presence of the oxide improves the wear resistance [29].

3.3 Corrosion behavior of $FeNiCrCoM_x$ HEAs

The corrosion behavior of the sintered $FeNiCrCoMi_x$ HEAs (where M=Si or Ti and x=0, 0.3, 0.6, and 0.9 wt.%) was investigated using 10% HCl, 10% HNO_3 or 10% H_2SO_4 solution.

3.3.1 Corrosion behavior in HCl solution

The effect of Si/Ti content on mass-loss due to the corrosion process of the sintered HEAs in 10% HCl shows two phenomena. The first is the lower mass-loss of all alloys containing Si than that of the base FeNiCrCo HEA. The second phenomenon is the increase in mass-loss value by increasing Si content. FeNiCrCoSi with 0.3 wt.% Si immersed in HCl solution has a low mass-loss and corrosion rate value of 8.743 mm/y, which has a lower corrosion rate than the base FeNiCrCo alloy (about 17.266 mm/y). In both $FeNiCrCoSi_{0.6}$ and $FeNiCrCoSi_{0.9}$ HEAs, the corrosion rate increases, which equals 11.917 mm/y and 13.300 mm/y, respectively. Although higher corrosion resistance of Si element with high hardness is got by increasing its content, some agglomerations are formed, which causes the formation of pores that facilitate the penetration of the corrosive medium (HCl) inside the alloy, and gives a good chance for its chemical reaction with the alloy. So, the corrosion rate increases and mass-loss also increases. Corrosion rates for $FeNiCrCoTi_x$ HEAs (x=0.3, 0.6, and 0.9 wt.%) are 11.888, 25.588, and 47.013 mm/y, respectively.

The corrosion behavior is affected by two parameters: the densification percentage and the chemical composition of the HEAs. As the densification percentage increases, the corrosion resistance also increases. From Fig. 6 and relative density results, the corrosion rate of the $FeNiCrCoTi_{0.3}$ HEA is lower than that of the FeNiCrCo HEA with almost the same densification percentage. It is lower than that of 0.3 wt.% Si, which has a higher density. So, the addition of 0.3 wt.% Ti improves the corrosion resistance of FeNiCrCo HEA. Increasing the Ti content leads to an increase in the densification percentage and a lower corrosion resistance than FeNiCrCo HEA in 10% HCl solution. This may be attributed to the affinity of Ti to oxygen, so by increasing Ti percentage with its good distribution in the alloy matrix, the chance for more corrosion increases.

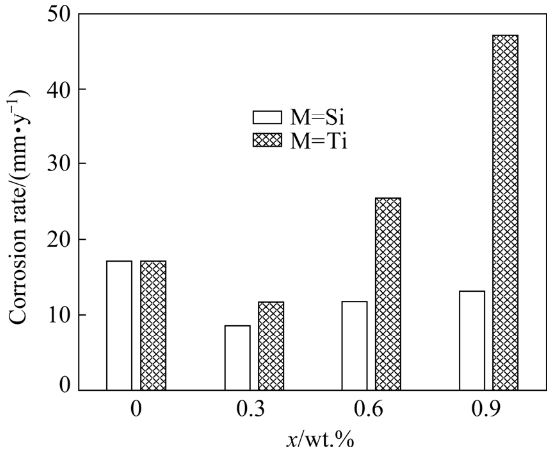

Fig. 6 Corrosion rates for $FeNiCrCoM_x$ HEAs (x=0, 0.3, 0.6, and 0.9 wt.%) immersed in 10% HCl solution

The SEM morphologies of the corroded surface of $FeNiCrCoSi_x$ and $FeNiCrCoTi_x$ HEAs (x=0.3, 0.6, and 0.9 wt.%) in 10% HCl solution are provided in Fig. 7. The EDX analysis results are tabulated in Tables 6 and 7, respectively. The lowest oxygen content of three $FeNiCrCoSi_x$ HEAs, from EDX results, was recorded for 0.3 wt.% Si, and the lowest oxygen content was recorded for 0.3 wt.% Ti

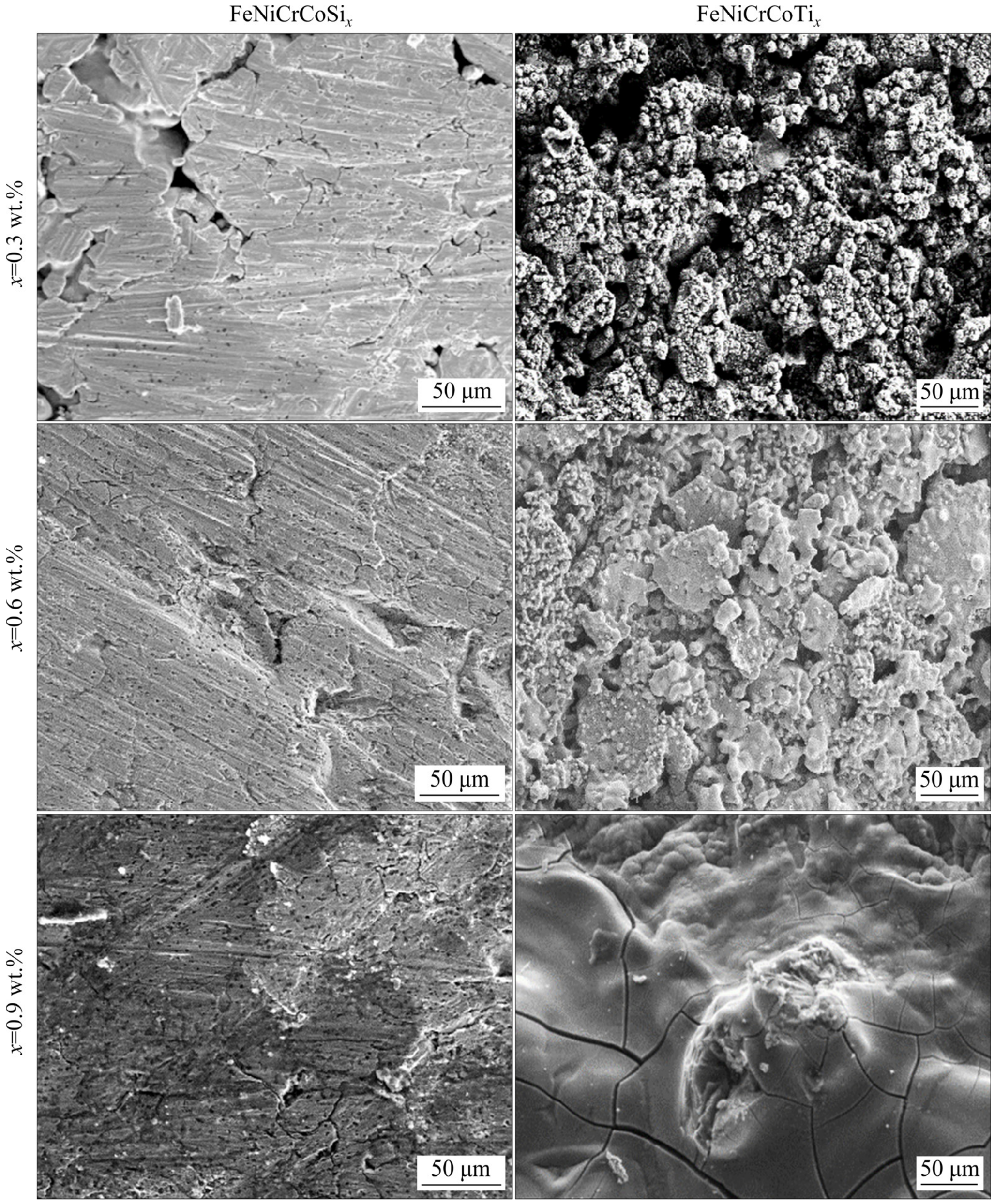

Fig. 7 SEM morphologies of corroded FeNiCrCoM$_x$ (M=Si or Ti) HEAs immersed in 10% HCl solution

Table 6 EDX results of corroded FeNiCrCoSi$_x$ (x=0.3, 0.6, and 0.9 wt.%) in 10% HCl, 10% HNO_3 and 10% H_2SO_4 solution (wt.%)

Element	FeNiCrCoSi$_{0.3}$			FeNiCrCoSi$_{0.6}$			FeNiCrCoSi$_{0.9}$		
	HCl	HNO_3	H_2SO_4	HCl	HNO_3	H_2SO_4	HCl	HNO_3	H_2SO_4
O	5.7	1.1	7.4	15.1	3.6	9.5	29.7	2.1	18.5
Fe	22.3	24.8	22.9	12.8	22.2	20.9	17	23.7	5.1
Ni	23.9	20.9	23.4	13.4	23.3	20.3	12.4	21.2	2.7
Cr	21.5	25.8	18.8	33.3	22.3	24.2	14.5	24.2	61.2
Co	25.6	26.1	25.9	16	25	23.1	14.2	25.1	3.9
Si	0.7	1	0.7	8.8	2.1	1	8.3	1.8	6.2
Cl	0.3	−	−	0.7	−	−	3.9	−	−
N	−	0.2	−	−	1.6	−	−	1.9	−
S	−	−	0.9	−	−	1	−	−	2.5

Table 7 EDX results of corroded FeNiCrCoTi$_x$ (x=0.3, 0.6, and 0.9 wt.%) immersed in 10% HCl, 10% HNO_3 and 10% H_2SO_4 solutions (wt.%)

Element	FeNiCrCoTi$_{0.3}$			FeNiCrCoTi$_{0.6}$			FeNiCrCoTi$_{0.9}$		
	HCl	HNO_3	H_2SO_4	HCl	HNO_3	H_2SO_4	HCl	HNO_3	H_2SO_4
O	9.9	3.2	5.8	13.4	4.1	8.9	26.9	11.2	12.7
Fe	27.7	18.7	19.1	21.2	23	22.6	19.5	11.3	20.2
Ni	20.8	19.7	23.3	21.9	19.1	22.7	21.2	4.8	26.4
Cr	18	33.2	24.1	18.6	25.7	19	11.3	54.6	14.6
Co	23.1	22.9	27	24.4	21.8	26.1	20.6	12.6	25.1
Ti	0.3	0.4	0.3	0.3	0.4	0.59	–	1	0.5
Cl	0.2	–	–	0.3	–	–	0.6	–	–
N	–	2	–	–	6	–	–	4.5	–
S	–	–	0.3	–	–	–	–	–	0.4

in a 10% HCl solution. This may be attributed to the low porosity of these samples and to the good homogeneity of both Si and Ti on the samples, which causes the good resistance to corrosion.

3.3.2 Corrosion behavior in HNO_3 solution

The effects of immersion time on the mass-loss of the three different HEAs immersed in 10% HNO_3 solution for 120 h at 20 °C was investigated. FeNiCrCoSi$_x$ HEA undergoes an increase in corrosion protection by increasing the Si content. The values of corrosion rate for FeNiCrCoSi$_x$ HEAs (x=0, 0.3, 0.6, and 0.9 wt.%) are equal to 6.561, 4.462, 3.204, and 3.3319 mm/y, respectively. This may also be attributed to the good corrosion resistance of Si with its ceramic nature and its low density, which causes its flotation on the sample surface and increases the corrosion resistance. However, by increasing the Si content, some agglomerations take place that cause the formation of pores, which consequently increases the corrosion rate. Corrosion rates for FeNiCrCoTi$_x$ HEAs (x=0.3, 0.6, and 0.9 wt.%) are 3.433, 14.1806, and 48.734 mm/y, respectively. Also, increasing the Ti content leads to an increase in the corrosion rate in 10% HNO_3 solution. This may be explained by the gradual increase of the porosity, since Ti has a very high melting point that causes immiscibility of it with other alloying elements, and consequently some agglomerations take place leading to a small sites for localized galvanic corrosion which increase the corrosion rate. According to Table 2 and Fig. 8, the corrosion rates of FeNiCrCoTi$_{0.3}$ HEA and FeNiCrCoSi$_{0.6}$ HEA are nearly equal, despite the fact that FeNiCrCoSi$_{0.6}$ HEA has a higher density. Then, FeNiCrCoSi$_{0.3}$ HEA also has good corrosion resistance.

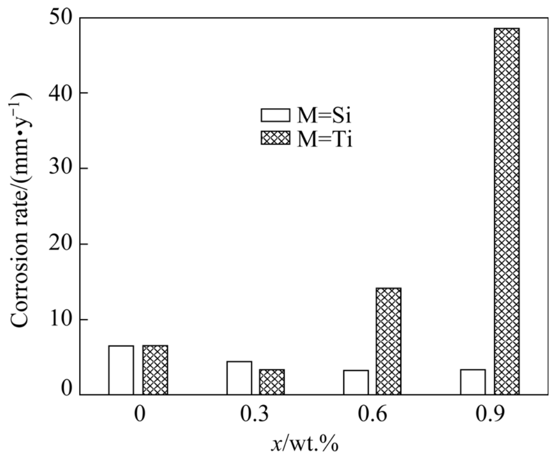

Fig. 8 Corrosion rates for FeNiCrCoM$_x$ HEAs (x=0, 0.3, 0.6, and 0.9 wt.%) immersed in 10% HNO_3 solution

In Fig. 9, the SEM morphologies of the corroded FeNiCrCoSi$_x$ and FeNiCrCoTi$_x$ HEAs (x=0.3, 0.6, and 0.9 wt.%) in HNO_3 solution are provided. The EDX results are given in Tables 6 and 7, respectively. A large number of small pits are observed in all HEAs, indicating a uniform corrosion of HEAs in HNO_3 solution.

3.3.3 Corrosion behavior in H_2SO_4 solution

The corrosion behavior of the sintered HEAs in 10% H_2SO_4 solution is plotted in Fig. 10. The corrosion rate of the FeNiCrCoSi$_x$ HEAs in H_2SO_4 solution is higher than that of FeNiCrCo HEA. The FeNiCrCoSi$_x$ HEAs (x=0, 0.3, 0.6, and 0.9 wt.%) have corrosion rate values of 8.232, 13.119, 27.039, and 39.839 mm/y, respectively. The corrosion rates of FeNiCrCoSi$_{0.6}$ and FeNiCrCoSi$_{0.9}$ HEAs are

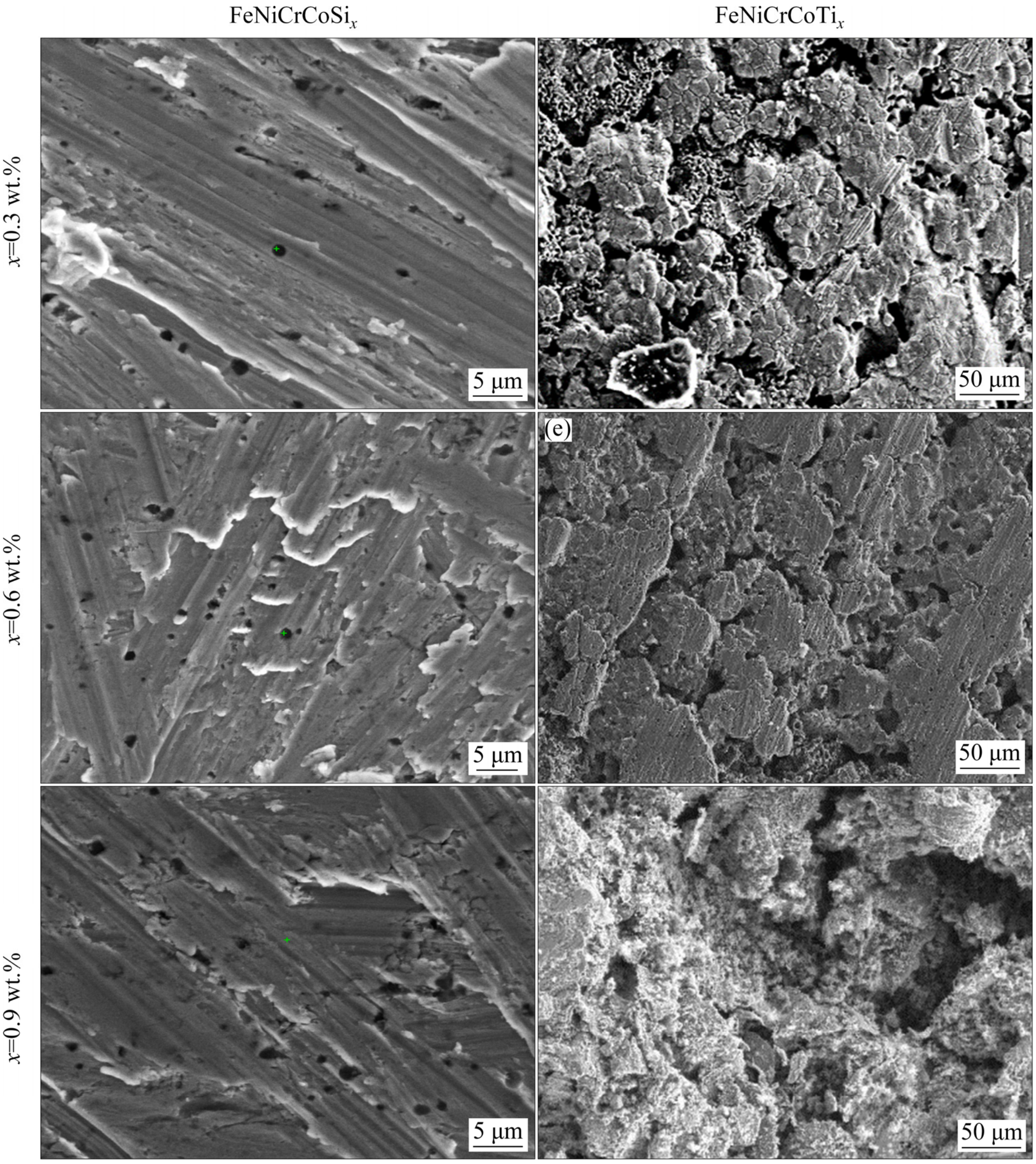

Fig. 9 SEM morphologies of corroded FeNiCrCoM$_x$ (M=Si or Ti) HEAs immersed in 10% HNO_3 solution

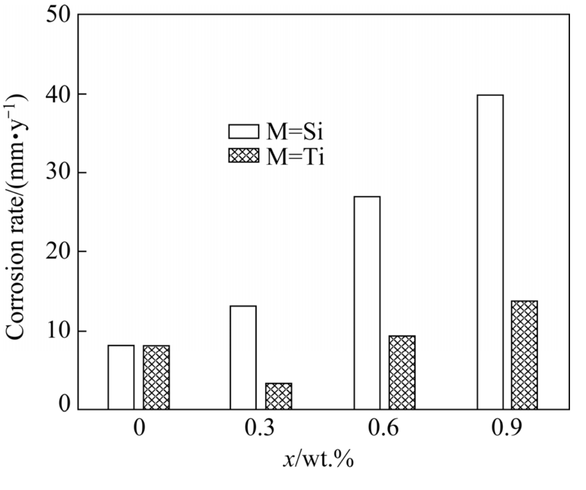

Fig. 10 Corrosion rates for FeNiCrCoM$_x$ HEAs (x=0, 0.3, 0.6, and 0.9 wt.%) immersed in 10% H_2SO_4 solution

high, as shown in Fig. 10. Corrosion rates for FeNiCrCoTi$_x$ HEAs (x=0.3, 0.6, and 0.9 wt.%) are 3.3007, 9.41, and 13.905 mm/y, respectively. Increasing the Ti content leads to an increase in the corrosion rate, but with the lower value in 10% H_2SO_4 than in 10% HCl and 10% HNO_3 solutions. As a result, the FeNiCrCoTi$_x$ HEAs outperform the FeNiCrCoSi$_x$ HEAs in 10% H_2SO_4 solution.

The SEM morphologies of the corroded FeNiCrCoSi$_x$ and FeNiCrCoTi$_x$ HEAs (x=0.3, 0.6, and 0.9 wt.%) in H_2SO_4 solution are provided in Fig. 11. EDX results of corroded FeNiCrCoSi$_x$ and FeNiCrCoTi$_x$ HEAs (x=0.3, 0.6, and 0.9 wt.%) in H_2SO_4 solution are provided in Tables 6 and 7, respectively. Large continuous pits are present in

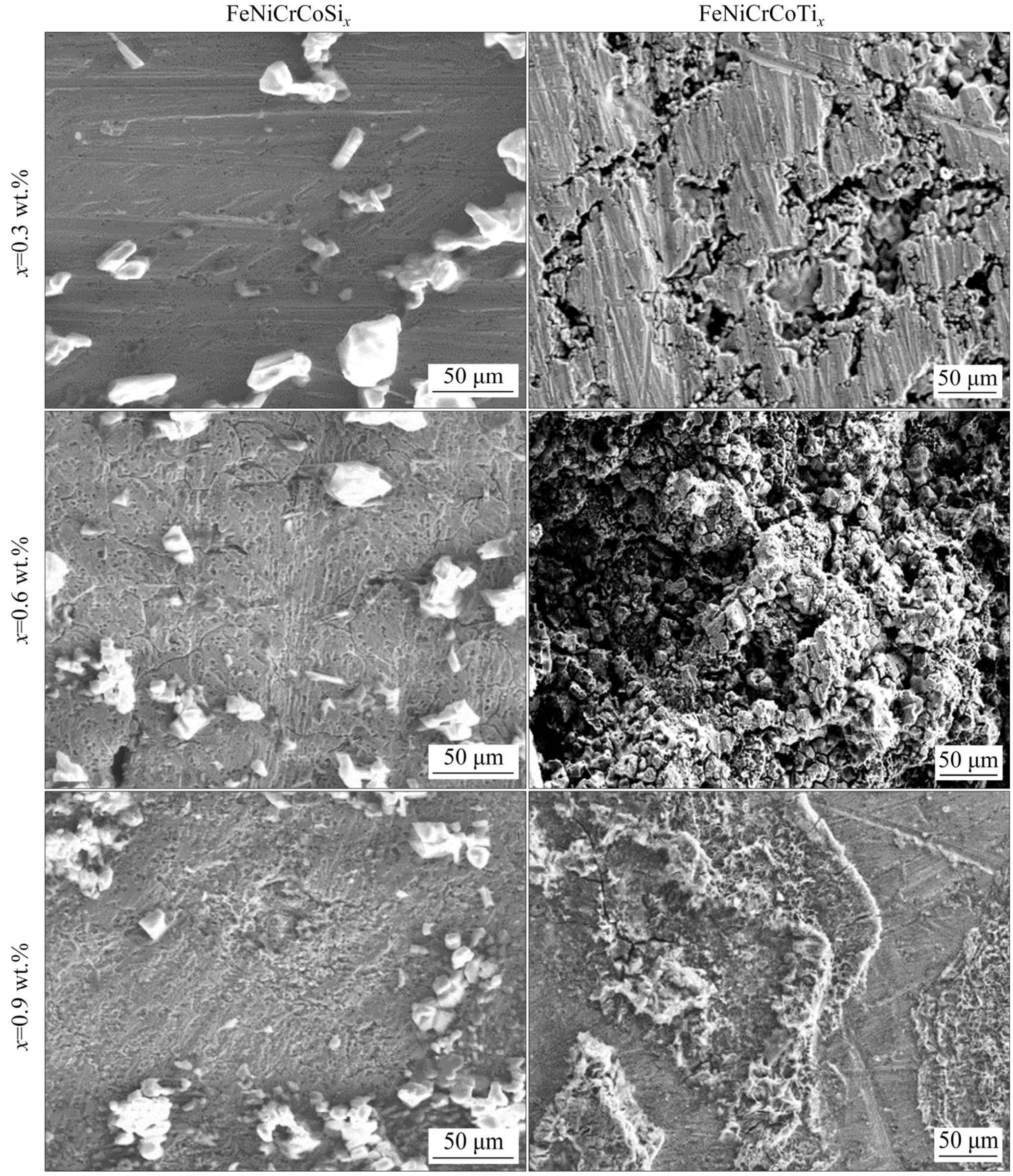

Fig. 11 SEM morphologies of corroded FeNiCrCoM$_x$ (M=Si or Ti) HEAs immersed in 10% H_2SO_4 solution

the middle of the HEA with 0.3 wt.% Si, where the 0.6 and 0.9 wt.% Si samples have numerous middle-sized pits in large amounts along their surfaces. Increasing the Ti content leads to an increase in the corrosion rate.

3.3.4 Discussion

The effect of Si on the corrosion behavior of FeNiCrCoSi$_x$ HEAs (x=0, 0.3, 0.6, and 0.9 wt.%) was investigated by using immersion in corrosive media of 10% HCl, 10% HNO_3, and 10% H_2SO_4 for 120 h. From all the above results, there are two phenomena. The first is the lower corrosion rate of 8.743 mm/y for FeNiCrCoSi$_{0.3}$ HEA in 10% HCl, while the highest rate of 39.839 mm/y for FeNiCrCoSi$_{0.9}$ HEA in 10% H_2SO_4. The second phenomenon is the lower corrosion rate of all alloys in 10% HNO_3 than in other acidic solutions. The effects of the immersion time on the mass-loss of the investigated alloys in H_2SO_4, HCl, and HNO_3 solutions show that the breakdown of all alloys is associated with general corrosion. The superior corrosion behavior is due to the locally disordered chemical environment caused by the random arrangement in a solid solution of multi-principal elements [35,36]. Despite the technological ability, the HEA preparation process is usually a challenge. Most HEAs suffer from inferior flowability or formability in the liquid state and therefore cannot be developed by traditional production routes into useful components [37]. The results generally show that $FeNiCrCoSi_{0.9}$ HEA has the highest corrosion rate and mass-reduction in the 10% H_2SO_4 corrosive medium, while FeNiCrCo HEA has the highest mass-reduction and corrosion rate in both HCl and HNO_3 solutions.

The dissolution of $FeNiCrCoSi_x$ (x=0, 0.3, 0.6, and 0.9 wt.%) HEAs in the beginning takes place due to the corrosion behavior of the acids. However, as a result of the dissolution, the formation of an oxide layer also occurs on the surface of the $FeNiCrCoSi_x$ (x=0, 0.3, 0.6, and 0.9 wt.%) HEAs. This oxide layer remains intact and inert in HNO_3, leading to the passivation of the HEAs plates, whereas in H_2SO_4 it starts to dissolve, resulting in a large corrosion rate. Hence, HCl and HNO_3 can be used for passivation of $FeNiCrCoSi_x$ only up to 48 and 96 h, respectively. Beyond that, it fails to protect the HEAs from corrosion. The results demonstrates that the Si addition greatly increases the corrosion resistance of the alloys in concentrated HNO_3 solution. The Si addition also increases the stability of the formed passive film on 0.6 wt.% Si sample relative to FeNiCrCo HEA. The dissolution rate of 0.6 wt.% Si and 0.9 wt.% Si samples can also be found to be higher than that of the 0.3 wt.% Si sample in H_2SO_4, and oxygen evolution occurs. The Cr and Si-depletion regions induced by precipitates enriched in Cr and Si in the 0.6 and 0.9 wt.% Si samples may be correlated with the elevated dissolution rate [38,39].

The corrosion behavior of $FeNiCrCoSi_x$ HEAs has been observed and compared in three different media. The corrosion resistance of $FeNiCrCoSi_x$ HEAs depends on the passive film or protective ability of microstructure [40]. The passive film formed on the 0.3 wt.% Si sample is strong enough to withstand weak corrosive media such as HNO_3 solution by immersion, morphology, and EDX results. The corrosion behavior of the $FeNiCrCoSi_x$ HEAs was investigated and compared with three different media. The corrosion (or dissolution) rate, however, is very quick once the passive film, which is actively corroded in the H_2SO_4 solution, is destroyed. This could be caused by the higher $Cr_2O_3/Cr(OH)_3$ ratio and the incorporation of Si oxides into the passive film of 0.3 wt.% Si sample, which improves passive film resistance to chloride attack. The corrosion resistance of 0.6 and 0.9 wt.% Si samples in H_2SO_4, however, depends on the weak sites induced by Cr and Si enriched precipitates. The areas around the precipitates in the matrix of 0.6 and 0.9 wt.% Si HEAs are depleted in Si and Cr, resulting in electrochemical activation at these locations. Therefore, the electrochemical attack is caused by 0.6 and 0.9 wt.% Si in HEAs regions depleted in Cr and Si serving as initiation sites. The corrosion activity of $FeNiCrCoSi_x$ HEAs is also altered by high-possibility precipitation. Pitting occurs in HEAs with single-phase and 0.3 wt.% Si, but preferentially localized corrosion occurs in HEAs with 0.6 and 0.9 wt.% Si [35]. The Si addition not only significantly increases the mechanical strength due to the solid solution of the Si material and the reinforcement of a nanoscale cellular structure by precipitation, but also decreases the ductility [41].

Increasing the Ti content leads to decreasing the powder particle size because of increasing the intrinsic strength of the HEAs by Ti additions. The solid solution strengthening increases by increasing the atomic size by Ti additions. This causes the strengthening of the FCC matrix but a decrease in its plasticity. Consequently, the powders have a lower tendency to agglomerate, resulting in a smaller particle size. There are two phenomena by increasing Ti. First, the increase in the Ti addition has a positive influence on the densification rate of $FeNiCrCoTi_x$ HEAs since an alloy with the least Ti ($FeNiCrCoTi_{0.3}$ HEA) shows the largest porosity. This can be caused by a decrease in melting temperature by Ti, which promotes densification process. The increase in strength associated with grain boundary strengthening can be neglected due to the relatively narrow range of obtained grain sizes [42]. This is in good agreement with the increasing hardness of Ti additions [43]. In all corrosive media, the $FeNiCrCoTi_{0.3}$ HEA has the highest corrosion resistance. It has good corrosion behavior especially in 10% HNO_3 and 10% H_2SO_4. Because of the second phenomenon, the increase in Ti additions leads to an increase in the agglomerations of the grey phase, as seen in Fig. 4, which affects the corrosion resistance by adding some local galvanized sits inside the HEAs to increase the corrosion rate.

4 Conclusions

(1) Homogenous distributions for all phases are observed in HEAs and some agglomerations are

found with high fractions. Si and Ti additions result in the formation of the FCC and BCC phases.

(2) All FeNiCrCoSi$_x$ HEAs are nearly fully densified with the Si additions, but the density for FeNiCrCoTi$_x$ HEAs is lower.

(3) The hardness is improved by different additions, either of Si or Ti. The wear rate is reduced by adding Si or Ti additions, which have lower wear rates than FeNiCrCo HEA.

(4) It can be concluded that the FeNiCrCoSi$_x$ (x=0.3, 0.6, and 0.9 wt.%) in 10% HNO$_3$ acid solution shows the highest corrosion resistance compared to 10% H$_2$SO$_4$ and 10% HCl media. However, FeNiCrCoTi$_x$ (x=0.3, 0.6, and 0.9 wt.%) has the highest corrosion resistance in 10%H$_2$SO$_4$ of all corrosive media.

(5) The corrosion behavior of FeNiCrCo HEA with additions of 0.3 wt.% Si/Ti in all corrosive media is the best. The surface morphologies of the corroded HEAs have a uniform corrosion and localized pitting with different sizes according to the corrosive medium. Generally, the best microstructure with a lower number of pits and small sizes is for HEAs with 0.3 wt.% Si.

References

[1] HSU Y C, LI C L, HSUEH C H. Effects of Al addition on microstructures and mechanical properties of CoCrFeMnNiAl$_x$ high entropy alloy films [J]. Entropy, 2020, 22(2): 1−11.

[2] CHENG C Y, YEH J W. High-entropy BNbTaTiZr thin film with excellent thermal stability of amorphous structure and its electrical properties [J]. Materials Letters, 2016, 185: 456−459.

[3] SHENG Wen-jie, YANG Xiao, WANG Cong, ZHANG Yong. Nano-crystallization of high-entropy amorphous NbTiAlSiW$_x$N$_y$ films prepared by magnetron sputtering [J]. Entropy, 2016, 18: 226.

[4] TANG Zhi, HUANG Lu, HE Wei, LIAW P. Alloying and processing effects on the aqueous corrosion behavior of high-entropy alloys [J]. Entropy, 2014, 16: 895−911.

[5] LUO Hong, LI Zhi-ming, MINGERS A, RAABE D. Corrosion behavior of an equiatomic CoCrFeMnNi high-entropy alloy compared with 304 stainless steel in sulfuric acid solution [J]. Corrosion Science, 2018, 134: 131−139.

[6] HUS C Y, SHEU T S, YEH J W, CHEN P H. Effect of iron content on wear behavior of AlCoCrFe$_x$Mo0.5Ni high-entropy alloys [J]. Wear, 2010, 268: 653−659.

[7] YE You-xiong, LIU Chen-ze, WANG Hai-jia, NIEH T G. Friction and wear behavior of a single-phase equiatomic TiZrHfNb high-entropy alloy studied using a nanoscratch technique [J]. Acta Materialia, 2018, 147: 78−89.

[8] ABOLKASSEM S, MOHAMED L, GABER G, ELKADY O. Microstructure and corrosion behavior of FeNiCoCrCu and FeNiCoCrMn high entropy alloys manufactured by powder metallurgy in different acid media [J]. Journal of Materials Research and Technology, 2021, 10: 1122−1142.

[9] WANG C, LI T H, LIAO Y C, LI C L, JANG J, HSUEH C H. Hardness and strength enhancements of CoCrFeMnNi high-entropy alloy with Nd doping [J]. Materials Science and Engineering A, 2019, 764: 138192.

[10] SCHUH B, FRANCISCA M, VOLKER B, GEORGE E, CLEMENS H, PIPPAN R, HOHENWARTER A. Mechanical properties, microstructure and thermal stability of a nanocrystalline CoCrFeMnNi high-entropy alloy after severe plastic deformation [J]. Acta Materialia, 2015, 96: 258−268.

[11] HE J Y, WANG H, HUANG H L, XU X D, CHEN M W, WU Y, LIU X J, NIEH T G, AN K, LU Z P. A precipitation-hardened high-entropy alloy without standing tensile properties [J]. Acta Materialia, 2016, 102: 187−196.

[12] KUMAR A, DHEKAR P, SWARNAKAR A, CHOPKAR M. Analysis of Si addition on phase formation in AlCoCrCuFeNiSi$_x$ high entropy alloys [J]. Materials Letters, 2017, 188: 73−76.

[13] LIU Xiao-tao, LEI Wen-bin, MA Li-juan, LIU Jing, LIU Jin-ling, CUI Jian-zhong. On the microstructures, phase assemblages and properties of Al0.5CoCrCuFeNiSi$_x$ high-entropy alloys [J]. Journal of Alloys and Compounds 2015, 630: 151−157.

[14] GUO S, NG C P, LU J, LIU C T. Effect of valence electron concentration on stability of fcc or bcc phase in high entropy alloys [J]. Journal of Applied Physics 2011, 109(10). Doi: 10.1063/1.3587228.

[15] TAKEUCHI A, AMIYA K, WADA T, YUBUTA K, ZHANG Wei, MAKINO A. Entropies in alloy design for high-entropy and bulk glassy alloys [J]. Entropy, 2013, 15: 3810−3821.

[16] ZHANG Bing-lin, FU Zheng-yi, ZHANG Jin-yong, WANG Wei-min, LEE S W, NIIHARA K. Characterization of nanocrystalline CoCrFeNiTiAl high- entropy solid solution processed by mechanical alloying [J]. Journal of Alloys and Compounds 2010, 495: 33−38.

[17] LIU Shao-fei, LIN Wei-tong, ZHAO Yi-lu, CHEN Da, YELI G, HE Feng, ZHAO Shi-jun, KAI J J. Effect of silicon addition on the microstructures, mechanical properties and helium irradiation resistance of NiCoCr-based medium-entropy alloys [J]. Journal of Alloys and Compounds, 2020, 844: 156162.

[18] JEONG K, JIN J E, JUNG Y S, KANG S, LEE Y K. The effects of Si on the mechanical twinning and strain hardening of Fe−18Mn−0.6C twinning-induced plasticity steel [J]. Acta Materialia, 2013, 61: 3399−3410.

[19] LEE S M, LEE S J, LEE S, NAM J H, LEE Y K. Tensile properties and deformation mode of Si-added Fe−18Mn−0.6C steels [J]. Acta Materialia, 2018, 144: 738−747.

[20] MORAAVCIK I, GAMANOV Š, MORAVCIKOVA-GOUVEA L, KOVACOVA Z, KITZMANTAL M, NEUBAUER E, DLOUHY I. Influence of Ti on the tensile properties of the high-strength powder metallurgy high entropy alloys [J]. Materials, 2020, 13: 578.

[21] MOHAMED L, ELKADY O, LOTFY M, AHMED H, ELREFAIE F. Characteristics of Ni−Cr binary alloys produced by conventional powder metallurgy [J]. Key Engineering Materials, 2019, 835: 214−222.

[22] MOHAMED L, GHANEM W, ELKADY O, LOTFY M, AHMED H, ELREFAIE F. Oxidation behavior of porous Ni-4 and 8 wt.% Cr alloys in air at 1273 K [J]. Egyptian Journal of Chemistry, 2020, 63(10): 3735−3745.

[23] ALY H, ABDELGHAFAR K, GABER G, MOHAMED L. Fabrication, characterization, and corrosion behavior of a new Cu40Mn25Al20Fe5Co5Ni5 high-entropy alloy in HNO_3 solution [J]. Journal of Materials Engineering and Performance, 2021, 30(1).

[24] MOHAMED L, GEPREEL M, ABDELFATAH A. Corrosion behavior of Al12Cr12Fe35Mn21Ni20 high entropy alloy in different acidic media [J]. Chemical Papers, 2021.

[25] MOHAMED L, HAMDY G, GABER G. Performance of GO/SiO_2, GO/TiO_2, and GO/ZrO_2 nanocomposites coatings as a corrosion barrier layer on AlSi−Cu−Mg Alloy in 3.5% NaCl solution [J]. International Journal of Electrochemical Science, 2021, 16: 210515.

[26] LIN Dan-yang, XU Lian-yong, LI Xiao-jie, JING Hong-yang, QIN Gang, PANG Hong-ning, MINAMI F. A Si-containing FeCoCrNi high-entropy alloy with high strength and ductility synthesized in situ via selective laser melting [J]. Additive Manufacturing, 2020, 35: 101340.

[27] LIU Hao, ZHANG Tong, SUN Shi-feng, ZHANG Guo-zhong, TIAN Xian-hue, CHEN Pei-jian. Microstructure and dislocation density of $AlCoCrFeNiSi_x$ high entropy alloy coatings by laser cladding [J]. Materials Letters, 2021, 283: 128746.

[28] PENG Shi-bo, LU Zheng. Effect of Y_2O_3/Ti/Zr addition on microstructureand hardness of ODS-CoCrFeNi HEAs produced by mechanical alloying and spark plasma sintering [J]. Journal of Alloys and Compounds, 2021, 861: 157940.

[29] WU Ming-yu, CHEN Ke, XU Zhen, LI D Y. Effect of Ti addition on the sliding wear behavior of AlCrFeCoNi, high-entropy alloy [J]. Wear, 2020, 462−463: 203493.

[30] ERDOGAN A, MERT K, ZEYTIN S. Effect of laser re-melting on electric current assistive sintered $CoCrFeNiAl_xTi_y$ high entropy alloys: Formation, micro-hardness and wear behaviors [J]. Surface and Coating Technology, 2020, 399: 125179.

[31] CHANG H, ZHANG T W, MA S G, ZHAO D, XIONG R L, WANG T, LI Z Q, WANG Z H. Novel Si-added CrCoNi medium entropy alloys achieving the breakthrough of strength−ductility trade-off [J]. Materials and Design, 2021, 197: 109202.

[32] TONG Y, CHEN D, HAN B, WANG J, FENG R, YANG T, ZHAO C, ZHAO Y L, GUO W, SHIMIZU Y, LIU C T, LIAW P K, INOUE K, NAGAI Y, HU A, KAI J J. Outstanding tensile properties of a precipitation-strengthened FeCoNiCrTi0.2 high-entropy alloy at room and cryogenic temperatures [J]. Acta Materialia, 2018, 165: 223−240.

[33] SAMSONOV G V. Mechanical properties of the elements. handbook of the physicochemical properties of the elements [M]. New York: Springer IFI-Plenum, 1968: 432.

[34] SHAHMIR H, NILI-AHMADABADI M, SHAFIE A, LANGDON T. Effect of a minor titanium addition on the super plastic properties of a CoCrFeNiMn high-entropy alloy processed by high pressure torsion [J]. Material Science and Engineering A, 2018, 718: 468−476.

[35] SHI Yun-zhu, YANG Bin, LIAW P. Corrosion-resistant high entropy alloys: A review [J]. Metals, 2017, 7(2): 43.

[36] DIAO Hao-yan, SANTODONATO L, TANG Zhi, EGAMI T, LIAW P. Local structures of high-entropy alloys (HEAs) on atomic scales: An overview [J]. The Journal of the Minerals, Metals & Materials Society, 2015, 67(10): 2321−2325.

[37] LU Yi-ping, DONG Yong, GUO Sheng, JIANG Li, KANG Hui-jun, WANG Tong-min, WEN Bin, WANG Zhi-jun, JIE J C, CAO Zhi-qiang, RUAN Hai-hui, LU Yi-ping. A promising new class of high-temperature alloys: Eutectic high-entropy alloys [J]. Scientific Reports, 2014, 4: 6200.

[38] SCHNEIDER M, KREMMER K, WEIDMANN S K, FURBETH W. Particle reinforced open porous anodizing layers on AA5005 [J]. Materials and Corrosion, 2017, 68: 1090−1098.

[39] CHEN Chen, ZHANG Hang, FAN Yan-zhou, WEI Ran, ZHANG Wei-wei, WANG Tan, ZHANG Tao, WU Kang, LI Fu-shan, GUAN Shao-kang, JIANG Jian-zhong. Improvement of corrosion resistance and magnetic properties of FeCoNiAl0.2Si0.2 high entropy alloy via rapid-solidification [J]. Intermetallics, 2020, 122: 106778.

[40] ZHAO Tian-liang, LIU Zhi-yong, DU Cui-wei, DAI Chun-duo, LI Xiao-gang. Corrosion fatigue crack initiation and initial propagation mechanism of E690 steel in simulated seawater [J]. Materials Science and Engineering A, 2017, 708: 181−192.

[41] CHAO Xiang, ZHANG Zhi, FU Hua-meng, HAN En-hou, ZHANG Hai-feng, WANG Jian-qiu. Microstructure and corrosion behavior of AlCoCrFeNiSi0.1 high-entropy alloy [J]. Intermetallics, 2019, 114: 106599.

[42] LABUSCH R A. A statistical theory of solid solution hardening [J]. Physica Status Solidi (b), 1970, 41(2): 659−669.

[43] MORAVCIKOVA-GOUVEA L, MORAVCIK I, OMASTA M, VESELÝ J, CIZEK J, MINÁRIK P, CUPERA J, ZÁDĚRA A, JAN V, DLOUHY I. High-strength $Al_{0.2}Co_{1.5}CrFeNi_{1.5}Ti$ high-entropy alloy produced by powder metallurgy and casting: A comparison of microstructures, mechanical and tribological properties [J]. Materials Characterization, 2019, 159: 110046.

添加 Si/Ti 对粉末冶金 FiNiCrCo 高熵合金物理力学和化学性能的影响

Sarah HEDYA[1], Lamiaa MOHAMED[2], Ghalia GABER[3],
Omayma ELKADY[4], Hassan MEGAHED[1], Shimaa ABOLKASSEM[4]

1. Mechanical Design and Production Engineering Department,
Faculty of Engineering, Cairo University, Giza 12613, Egypt;
2. Mining, Petroleum and Metallurgical Engineering Department,
Faculty of Engineering, Cairo University, Giza 12613, Egypt;
3. Department of Chemistry, Faculty of Science (Girls), Al-Azhar University,
P.O. Box: 11754, Yousef Abbas Str., Nasr City, Cairo, Egypt;
4. Powder Technology Division, Manufacturing Technology Institute,
Central Metallurgical R&D Institute, P.O. Box. 87, Helwan 11421, Cairo, Egypt

摘　要：用粉末冶金法制备 FiNiCrCoSi$_x$ 和 FiNiCrCoTi$_x$ 高熵合金(HEAs)。其中 x 为 0、0.3%、0.6%和 0.9%(质量分数)。所有合金中均形成均匀分布的固溶体。与 FiNiCrCo 高熵合金相比，加入 Si 和 Ti 后，合金的密度和硬度提高，研究合金在不同载荷下的磨损率。结果表明，含 0.3%Si 和 0.9%Ti 的高熵合金磨损率最低。用 XRD、SEM 和 EDX 研究 HEAs 的相组或、晶粒尺寸和显微组织。通过 H_2SO_4、HNO_3 和 HCl 溶液浸泡实验，研究 Si 和 Ti 含量对烧结态 FiNiCrCoSi$_x$ 和 FiNiCrCoTi$_x$ HEAs 腐蚀行为和表面形貌的影响。在样品表面观察到不同尺寸的均匀腐蚀和局部点蚀，且 FiNiCrCoSi$_{0.3}$ 合金具有更小，更少的蚀坑，和优异的显微组织

关键词：FiNiCrCoSi$_x$ 合金，FiNiCrCoTi$_x$ 合金；高熵合金，粉末冶金；腐蚀行为

(Edited by Bing YANG)